JACS
JOURNAL OF THE AMERICAN CHEMICAL SOCIETY
Communication
Cite This: J. Am. Chem. Soc. 2017, 139, 14360-14363
pubs.acs.org/JACS

# *Operando* Phonon Studies of the Protonation Mechanism in Highly Active Hydrogen Evolution Reaction Pentlandite Catalysts

Ioannis Zegkinoglou,[†] Ali Zendegani,[‡] Ilya Sinev,[†] Sebastian Kunze,[†] Hemma Mistry,[†,∥] Hyo Sang Jeon,[†] Jiyong Zhao,[⊥] Michael Y. Hu,[⊥] E. Ercan Alp,[⊥] Stefan Piontek,[#] Mathias Smialkowski,[#] Ulf-Peter Apfel,[#] Fritz Körmann,[‡] Jörg Neugebauer,[‡] Tilmann Hickel,*[,‡] and Beatriz Roldan Cuenya*[,†,▲]

[†]Department of Physics, Ruhr-University Bochum, 44780 Bochum, Germany
[‡]Max-Planck-Institut für Eisenforschung, 40237 Düsseldorf, Germany
[∥]Department of Physics, University of Central Florida, Orlando, Florida 32816, United States
[⊥]Advanced Photon Source, Argonne National Laboratory, Lemont, Illinois 60439, United States
[#]Inorganic Chemistry I, Ruhr-University Bochum, 44780 Bochum, Germany
[▲]Department of Interface Science, Fritz-Haber Institute of the Max Planck Society, 14195 Berlin, Germany

Supporting Information

**ABSTRACT:** Synthetic pentlandite ($Fe_{4.5}Ni_{4.5}S_8$) is a promising electrocatalyst for hydrogen evolution, demonstrating high current densities, low overpotential, and remarkable stability in bulk form. The depletion of sulfur from the surface of this catalyst during the electrochemical reaction has been proposed to be beneficial for its catalytic performance, but the role of sulfur vacancies and the mechanism determining the reaction kinetics are still unknown. We have performed electrochemical *operando* studies of the vibrational dynamics of pentlandite under hydrogen evolution reaction conditions using $^{57}Fe$ nuclear resonant inelastic X-ray scattering. Comparing the measured Fe partial vibrational density of states with density functional theory calculations, we have demonstrated that hydrogen atoms preferentially occupy substitutional positions replacing pre-existing sulfur vacancies. Once all vacancies are filled, the protonation proceeds interstitially, which slows down the reaction. Our results highlight the beneficial role of sulfur vacancies in the electrocatalytic performance of pentlandite and give insights into the hydrogen adsorption mechanism during the reaction.

The search for highly efficient hydrogen evolution reaction (HER) catalysts made of abundant, non-noble elements is of crucial importance for low-cost, sustainable hydrogen production for energy storage applications.[1] Platinum and its alloys remain unparalleled in their ability to yield high current densities at low overpotentials as HER catalysts,[2] but their high cost and low natural abundance significantly reduce the potential for large-scale implementation. Transition metal dichalcogenides have recently emerged as promising alternatives to precious metals, combining remarkable electrocatalytic performance with exceptional durability under harsh acidic or alkaline conditions.[3−7] While most of these cost-efficient catalysts require nanostructuring or surface modification to exhibit the desired catalytic properties, it was recently shown that synthetic bulk pentlandite ($Fe_{4.5}Ni_{4.5}S_8$) can yield high current densities (up to 650 mA $cm^{-2}$ at an overpotential of 0.6 V) and remarkable stability under acidic conditions in rock-like form.[8,9] Interestingly, the overpotential required for hydrogen evolution on this catalyst gradually decreases within a time span of several hours during the electrochemical reaction (from 280 to 190 mV after 96 h). Based on complementary XPS, SEM, and EDX characterization, this observation was tentatively attributed to the depletion of sulfur from the surface of the electrode,[8] but no understanding of the trend at the atomic level and its possible correlation to the electrocatalytic HER mechanism is available to date. Such an understanding is crucial for further tuning the properties of transition metal chalcogenide electrocatalysts.

In order to identify the role of sulfur vacancies in the catalytic performance of pentlandite and to shed light on the protonation mechanism on its surface, we performed nuclear resonant inelastic X-ray scattering (NRIXS) studies on powder pentlandite samples both in air and under *operando* HER conditions in an aqueous 0.5 M $H_2SO_4$ electrolyte. NRIXS directly probes lattice vibrations (phonons) in the near-surface (~500 nm probing depth at grazing incidence) region of the catalyst, which are highly sensitive to chemical adsorption and structural deformations. The Fe partial vibrational densities of states (VDOS) determined by NRIXS under different conditions with an energy resolution of ~1 meV were compared with theoretical phonon spectra obtained from first-principles calculations performed for various atomic configurations, involving different concentrations and different positions of sulfur vacancies and hydrogen atoms in the lattice. Based on this comparison we were able to shed light on the hydrogen adsorption process at the atomic level under reaction conditions.

The pentlandite powder in our study was synthesized from the elements, as previously reported.[8] It was not isotopically enriched. The NRIXS measurements were performed at

**Received:** July 27, 2017
**Published:** September 22, 2017






DOI: 10.1021/jacs.7b07902
J. Am. Chem. Soc. 2017, 139, 14360−14363

beamline 3ID-B of the Advanced Photon Source (Argonne, USA) at the X-ray photon energy corresponding to the nuclear resonance of $^{57}$Fe (14.413 keV) in a custom-made electrochemical cell (Figure S1 in Supporting Information, SI). Nuclear resonant fluorescence and atomic nonresonant fluorescence photons were detected simultaneously with an avalanche photodiode and subsequently separated with the help of timing electronics[10,11] (see SI). In-depth electrochemical characterization of an identically synthesized powder sample was previously reported.[8]

A large number of NRIXS spectra were acquired over a time frame of ~24 h for every experimental condition (see later in text) and summed up to achieve good quality statistics. The Fe partial VDOS was obtained from the NRIXS energy spectra (Figures S2–S4, SI) upon subtraction of the elastic peak at zero energy,[12−14] using a quasi-harmonic model with well-defined phonon states and multiphonon contributions in the PHOENIX software.[15] This technique has been previously used by our group to study the phonon dynamics of Fe and Fe-alloy nanoclusters,[16−18] as well as by others for a variety of material systems.[19−22] The resulting VDOS spectra are shown in Figure 1 for the pentlandite sample in air (as-prepared state)

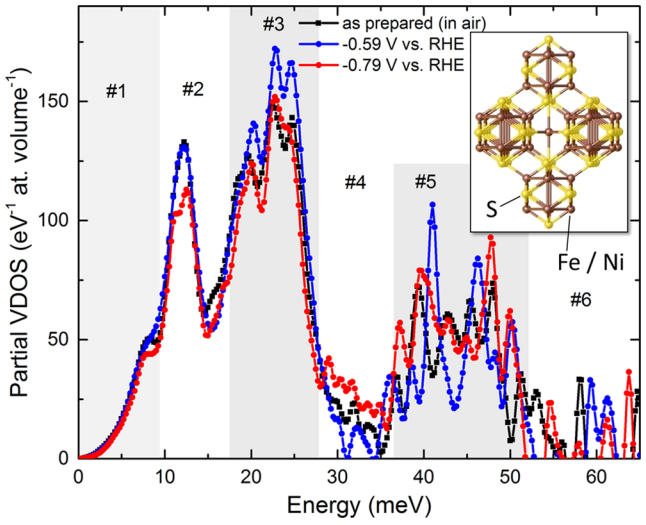


**Figure 1.** Experimental Fe partial vibrational density of states of pentlandite in air (black) and under *operando* HER conditions (blue at −0.59 V, and red at −0.79 V, both versus RHE) extracted from the phonon excitation NRIXS spectra. The inset shows the pentlandite structure.

and under *operando* HER conditions at two different applied potentials, −0.59 V and −0.79 V versus the reversible hydrogen electrode (RHE). Several thermodynamic and lattice dynamics parameters, such as the mean force constant, the kinetic energy per atom, and the vibrational specific heat, are obtained directly from the experimental VDOS and summarized in Table S1 (SI). Significant changes are observed in the relative intensities and energy positions of several spectral features upon electrochemical reduction. The changes are dependent on the applied potential and reflect variations both with respect to the adsorbate species that become bound to iron during the catalytic process (higher frequency optical modes) and with respect to cooperative, longer-range motions in the lattice (lower frequency modes).[23,24]

First-principles calculations were performed within the framework of density functional theory (DFT), using plane-wave basis sets as implemented in the Vienna ab initio simulation package (VASP)[25,26] and the Perdew–Burke–Ernzerhof (PBE)[27] exchange-correlation functional in the generalized gradient approximation (GGA). The calculated partial VDOS for Fe is shown in Figure 2a, for the case of a

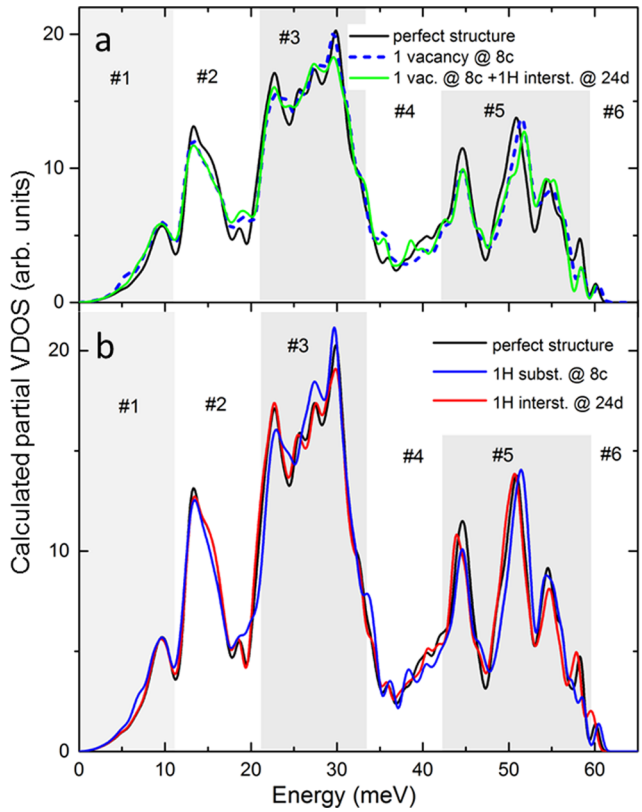


**Figure 2.** Theoretical Fe partial vibrational density of states in pentlandite obtained with DFT. (a) The effect of a H atom at interstitial site 24d (green) in the presence of a sulfur vacancy in the lattice (at Wyckoff position 8c). The effect of a S vacancy alone (dashed blue) is also shown in comparison with the VDOS of a perfect structure (black). (b) The VDOS of protonated lattices with one H atom at interstitial site Wyckoff 24d or substitutional 8c. The spectrum of a perfect pentlandite structure is shown for comparison.

perfect, defect-free supercell consisting of 136 atoms ($Fe_{36}Ni_{36}S_{64}$, black curve), as well as for a structure in which one of the sulfur atoms has been removed, leaving behind a vacancy at Wyckoff position 8c ($Fe_{36}Ni_{36}S_{63}$, dashed blue curve; see atomic positions in Figure S5, SI). The calculated VDOS of the H-free cell (Figure 2, black) and the experimental VDOS of the as-prepared sample (Figure 1) are in good agreement. All main characteristics of the NRIXS-derived spectrum acquired in air prior to the electrochemical reaction are well reproduced by the calculations. For example, the sharp, asymmetric feature at phonon energy around 12 meV (spectral region #2, Figure 1) preceded by a shoulder at 7.5 meV (#1), the four-peak structure between 18.5 and 25 meV (#3), and the weaker, partly overlapping peaks between 37 and 48 meV (#5) (all energy values referring to the experimental spectra) are clearly observed in the theoretical simulations. In the calculated VDOS, a slight overestimation of the phonon energy positions, resulting in a small "stretching" of the energy scale with respect to the experimental spectra, was observed. This is a well-known



DOI: 10.1021/jacs.7b07902
J. Am. Chem. Soc. 2017, 139, 14360−14363

effect caused by the underestimation of the volume of the crystal structure at room temperature (see SI).

In order to identify the position that the H atom occupies in the pentlandite lattice upon adsorption, we calculated the energy required for replacing a sulfur vacancy at Wyckoff position 8c or 24e with H. We further calculated the energy needed for adding H at an interstitial position (4a or 24d), in both the presence and absence of a sulfur vacancy. The calculations clearly demonstrate that, in the case of preexisting sulfur vacancies, the H atom prefers to occupy a former sulfur site at Wyckoff position 8c rather than an interstitial position, leading to a substitutional configuration. The energy of this arrangement is lower by 1.6 eV as compared to an interstitial configuration where the sulfur vacancy at site 8c remains unoccupied and the H atom occupies a lattice site 24d instead, and lower by 1.8 eV compared to a configuration where H occupies an interstitial site 4a. The H atom binding mechanism changes once the sulfur vacancy has been filled. Without a vacancy being available in the supercell, it is now favorable for the hydrogen atom to occupy the interstitial site 24d (energy lower by 0.15 eV as compared to site 4a), while it is unlikely to replace a sulfur atom at a substitutional position. The results of the energy calculations are summarized in Table S3 in the SI.

The above tentative conclusions are confirmed by comparing the calculated VDOS of the hydrogenated pentlandite (Figure 2) with that of a supercell containing no H atom, as well as with the experimental NRIXS-derived spectra (Figure 1). The addition of an H interstitial (green line in Figure 2a) into a supercell that contains a sulfur vacancy (dashed blue line in Figure 2a) changes the DOS only slightly, without reproducing some of the characteristic trends observed in the experimental spectrum. On the other hand, the addition of H as a substitutional atom (blue line, Figure 2b) in the former vacancy at Wyckoff position 8c has a remarkable effect in the VDOS. The latter results in a significant intensity increase of the two peaks around 28 meV (region #3 in the experimental spectra). Furthermore, the peak around 23 meV also shows an increase, while the minimum at 19 meV (region #2) and the shoulder at 35 meV (region #4) decrease. All these theoretical predictions are in agreement with the observed changes in the *operando* NRIXS spectra at applied potential −0.59 V vs RHE. Complete consistency with our experimental trend (in particular the increase of the two central peaks) cannot be obtained if only scenarios without sulfur vacancies are considered (Figure 3), indicating the importance of these defects.

The experimental trends are significantly different for the higher applied potential of −0.79 V vs RHE. The calculations support the hypothesis that in this case most of the sulfur vacancies are filled by H atoms. Using the vacancy-free structure as a reference, the effect of gradually adding up to eight H atoms to the supercell is shown in Figure 3 for substitutional (Figure 3a, $Fe_{36}Ni_{36}S_{64-x}H_x$) and interstitial (Figure 3b, $Fe_{36}Ni_{36}S_{64}H_x$) configurations. It is obvious that the substitutional protonation modifies the VDOS in ways which are not consistent with the experimental results. For example, the modes between 40 and 60 meV (#5) are strongly suppressed and the ratio of the dominant peaks between 20 and 30 meV (#3) is clearly modified, resulting in a flattened structure in this energy region, different from what was observed in the experiment upon applying a more negative potential. On the other hand, the assumption of a gradual filling with interstitial H atoms at Wyckoff positions 24d, once the

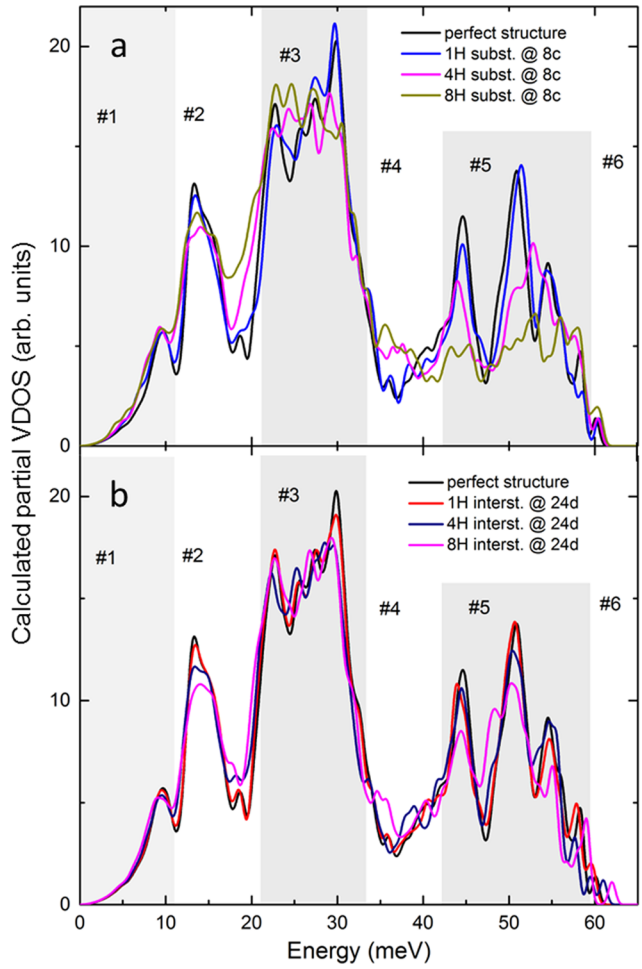


**Figure 3.** Theoretical Fe-projected vibrational density of states in pentlandite, assuming the presence of one, four or eight H atoms in the unit cell: (a) at substitutional Wyckoff positions 8c; (b) at interstitial Wyckoff positions 24d. The VDOS of a perfect structure is shown for comparison.

substitutional vacancy has been filled, reproduces all main features of the experimental spectra. Most importantly, the peak at 30 meV (region #3) was found to decrease, while the neighboring peak at 26 meV and the peak at 23 meV are almost unchanged. Alternative substitutional (24e) and interstitial (4a) positions were also systematically investigated and compared in the calculations. The corresponding calculated VDOS are shown in Figures S7 and S8 in the SI. No good agreement with the experimental trends is obtained for any of those configurations.

The above-mentioned results are consistent with the nonlinear dependence of the charge transfer resistance on the activation potential, as demonstrated by the electrochemical impedance spectroscopy measurements shown in Figure S10 (SI). It seems plausible that the occupation of the majority of sulfur vacancies by hydrogen atoms at a potential of about −0.6 V and the subsequent change of the protonation (from substitutional to interstitial) are responsible for the nonlinear alteration of the reaction kinetics. This is also reflected in the experimentally determined thermodynamic parameters (derived from NRIXS) shown in Table S1 (SI). Those exhibit a nonmonotonic trend, with either a local maximum or a local minimum at potential −0.59 V vs RHE. The promoting role of S vacancies suggested by NRIXS and DFT for the protonation



DOI: 10.1021/jacs.7b07902
J. Am. Chem. Soc. 2017, 139, 14360−14363

mechanism provides a viable explanation for the previously reported decrease with time of the onset potential under HER conditions (activation process):[8] the gradual depletion of S from the catalyst makes more vacancies available for substitutional H adsorption, which lowers the energy threshold of the process. The possibility that dissolved Pt from the counter electrode contributes to the decrease of the overpotential also needs to be considered for long-lasting electrochemical experiments. However, control measurements with alternative counter electrode materials showed that this effect is not a significant factor in our studies (see Figure S13 and related text in SI).

In conclusion, *operando* high energy resolution NRIXS studies and first-principles DFT calculations revealed the key role of sulfur vacancies in the catalytic HER performance of synthetic pentlandite. We showed that hydrogen atoms preferentially occupy sulfur vacancies at substitutional lattice sites (Wyckoff 8c) until all vacancies are filled. Afterward, the protonation proceeds with H atoms occupying interstitial positions (Wyckoff 24d). The occupation of alternative lattice sites by hydrogen is not energetically favorable. The results demonstrate the power of the combination of NRIXS with DFT when probing phonon dynamics, revealing valuable information on the dynamic nature of structural and surface properties of the acting catalyst during an electrocatalytic process.

## ■ ASSOCIATED CONTENT

### Supporting Information

The Supporting Information is available free of charge on the ACS Publications website at DOI: 10.1021/jacs.7b07902.

Methods, NRIXS spectra, additional VDOS calculations, thermodynamic parameters, electrochemical characterization (PDF)

## ■ AUTHOR INFORMATION


### Corresponding Authors

*Beatriz.Roldan@rub.de
*t.hickel@mpie.de

### ORCID

Hemma Mistry: 0000-0002-6065-3340
Beatriz Roldan Cuenya: 0000-0002-8025-307X


### Notes

The authors declare no competing financial interest.

## ■ ACKNOWLEDGMENTS

We thank Andrei V. Ruban for providing the spcm program for generating the special quasi-random structures. This work was funded by the US National Science Foundation (NSF-Chemistry 1213182, NSF-DMR 1207065) and the Deutsche Forschungsgemeinschaft (DFG) through the Cluster of Excellence RESOLV at RUB (EXC 1069). This research used resources of the Advanced Photon Source, a U.S. Department of Energy (DOE) Office of Science User Facility operated by Argonne National Lab. under Contract No. DE-AC02-06CH11357. U.-P.A. thanks the Fonds der Chemischen Industrie (FCI) (Liebig grant), and the DFG (Emmy Noether grant AP242/2-1) for financial support.

## ■ REFERENCES


(1) Vesborg, P. C. K.; Seger, B.; Chorkendorff, I. *J. Phys. Chem. Lett.* **2015**, *6*, 951.
(2) Yin, H.; Zhao, S.; Zhao, K.; Muqsit, A.; Tang, H.; Chang, L.; Zhao, H.; Gao, Y.; Tang, Z. *Nat. Commun.* **2015**, *6*, 6430.
(3) Kibsgaard, J.; Chen, Z.; Reinecke, B. N.; Jaramillo, T. F. *Nat. Mater.* **2012**, *11*, 963.
(4) Li, Y.; Wang, H.; Xie, L.; Liang, Y.; Hong, G.; Dai, H. *J. Am. Chem. Soc.* **2011**, *133*, 7296.
(5) Voiry, D.; Salehi, M.; Silva, R.; Fujita, T.; Chen, M.; Asefa, T.; Shenoy, V. B.; Eda, G.; Chhowalla, M. *Nano Lett.* **2013**, *13*, 6222.
(6) Tan, Y.; Liu, P.; Chen, L.; Cong, W.; Ito, Y.; Han, J.; Guo, X.; Tang, Z.; Fujita, T.; Hirata, A.; Chen, M. W. *Adv. Mater.* **2014**, *26*, 8023.
(7) Pandey, M.; Vojvodic, A.; Thygesen, K. S.; Jacobsen, K. W. *J. Phys. Chem. Lett.* **2015**, *6*, 1577.
(8) Konkena, B.; junge Puring, K.; Sinev, I.; Piontek, S.; Khavryuchenko, O.; Dürholt, J. P.; Schmid, R.; Tüysüz, H.; Muhler, M.; Schuhmann, W.; Apfel, U.-P. *Nat. Commun.* **2016**, *7*, 12269.
(9) junge Puring, K.; Piontek, S.; Smialkowski, M.; Burfeind, J.; Kaluza, S.; Doetsch, C.; Apfel, U.-P. *J. Visualized Exp.* **2017**, *124*, e56087.
(10) Alp, E. E.; Sturhahn, W.; Toellner, T. S.; Zhao, J.; Hu, M.; Brown, D. E. *Hyperfine Interact.* **2002**, *144*, 3.
(11) Röhlsberger, R. *J. Phys.: Condens. Matter* **2001**, *13*, 7659.
(12) Sturhahn, W.; Toellner, T. S.; Alp, E. E.; Zhang, X.; Ando, M.; Yoda, Y.; Kikuta, S.; Seto, M.; Kimball, C. W.; Dabrowski, B. *Phys. Rev. Lett.* **1995**, *74*, 3832.
(13) Chumakov, A. I.; Rüffer, R.; Grünsteudel, H.; Grünsteudel, H. F.; Grübel, G.; Metge, J.; Leupold, O.; Goodwin, H. A. *Europhys. Lett.* **1995**, *30*, 427.
(14) Chumakov, A. I.; Sturhahn, W. *Hyperfine Interact.* **1999**, *123*, 781.
(15) Sturhahn, W. *Hyperfine Interact.* **2000**, *125*, 149.
(16) Roldan Cuenya, B.; Croy, J. R.; Ono, L. K.; Naitabdi, A.; Heinrich, H.; Keune, W.; Zhao, J.; Sturhahn, W.; Alp, E. E.; Hu, M. *Phys. Rev. B: Condens. Matter Mater. Phys.* **2009**, *80*, 125412.
(17) Roldan Cuenya, B.; Naitabdi, A.; Croy, J.; Sturhahn, W.; Zhao, J.; Alp, E.; Meyer, R.; Sudfeld, D.; Schuster, E.; Keune, W. *Phys. Rev. B: Condens. Matter Mater. Phys.* **2007**, *76*, 195422.
(18) Roldan Cuenya, B.; Ono, L. K.; Croy, J. R.; Naitabdi, A.; Heinrich, H.; Zhao, J.; Alp, E. E.; Sturhahn, W.; Keune, W. *Appl. Phys. Lett.* **2009**, *95*, 143103.
(19) Mauger, L.; Lucas, M. S.; Muñoz, J. A.; Tracy, S. J.; Kresch, M.; Xiao, Y.; Chow, P.; Fultz, B. *Phys. Rev. B: Condens. Matter Mater. Phys.* **2014**, *90*, 064303.
(20) Fultz, B. *Prog. Mater. Sci.* **2010**, *55*, 247.
(21) Kamali, S.; Wang, H.; Mitra, D.; Ogata, H.; Lubitz, W.; Manor, B. C.; Rauchfuss, T. B.; Byrne, D.; Bonnefoy, V.; Jenney, F. E.; Adams, M. W. W.; Yoda, Y.; Alp, E.; Zhao, J.; Cramer, S. P. *Angew. Chem., Int. Ed.* **2013**, *52*, 724.
(22) Couet, S.; Schlage, K.; Diederich, T.; Rüffer, R.; Theis-Bröhl, K.; Toperverg, B. P.; Zhernenkov, K.; Zabel, H.; Röhlsberger, R. *New J. Phys.* **2009**, *11*, 013038.
(23) Rai, B. K.; Durbin, S. M.; Prohofsky, E. W.; Sage, J. T.; Ellison, M. K.; Roth, A.; Scheidt, W. R.; Sturhahn, W.; Alp, E. E. *J. Am. Chem. Soc.* **2003**, *125*, 6927.
(24) Li, J.; Peng, Q.; Oliver, A. G.; Alp, E. E.; Hu, M. Y.; Zhao, J.; Sage, J. T.; Scheidt, W. R. *J. Am. Chem. Soc.* **2014**, *136*, 18100.
(25) Kresse, G.; Furthmüller, J. *Phys. Rev. B: Condens. Matter Mater. Phys.* **1996**, *54*, 11169.
(26) Kresse, G.; Hafner, J. *Phys. Rev. B: Condens. Matter Mater. Phys.* **1993**, *47*, 558.
(27) Perdew, J. P.; Burke, K.; Ernzerhof, M. *Phys. Rev. Lett.* **1996**, *77*, 3865.




DOI: 10.1021/jacs.7b07902
J. Am. Chem. Soc. 2017, 139, 14360−14363